

Strong bulk spin-orbit torques quantified in the van der Waals ferromagnet Fe_3GeTe_2

Franziska Martin¹, Kyujoon Lee^{1,2,‡}, Maurice Schmitt¹, Anna Liedtke¹, Aga Shahee¹, Haakon Thømt Simensen³, Tanja Scholz⁴, Tom G. Saunderson¹, Dongwook Go⁵, Martin Gradhand^{1,6}, Yuriy Mokrousov^{1,5}, Thibaud Denneulin⁷, András Kovács⁷, Bettina Lotsch⁴, Arne Brataas³, Mathias Kläui^{1,3}

¹Institute of Physics, Johannes Gutenberg-University, 55099 Mainz, Germany

²Division of Display and Semiconductor Physics, Korea University, 30019 Sejong, Korea

³Centre for Quantum Spintronics, Department of Physics, Norwegian University of Science and Technology, 7491 Trondheim, Norway

⁴Max Planck Institute for solid state research, 70569 Stuttgart, Germany

⁵Peter Grünberg Institut and Institute for Advanced Simulation, Forschungszentrum Jülich and JARA, 52425 Jülich, Germany

⁶H. H. Wills Physics Laboratory, University of Bristol, Bristol BS8 1TL, United Kingdom

⁷Ernst Ruska-Centre for Microscopy and Spectroscopy with Electrons and Peter Grünberg Institute, Forschungszentrum Jülich, 52425 Jülich, Germany

[‡]Author to whom correspondence should be addressed: kyulee@uni-mainz.de

Abstract

The recent emergence of magnetic van der Waals materials allows for the investigation of current induced magnetization manipulation in two dimensional materials. Uniquely, Fe_3GeTe_2 has a crystalline structure that allows for the presence of *bulk* spin-orbit torques (SOTs), that we quantify in a Fe_3GeTe_2 flake. From the symmetry of the measured torques, we identify the current induced effective fields using harmonic analysis and find dominant *bulk* SOTs, which arise from the symmetry in the crystal structure. Our results show that Fe_3GeTe_2 uniquely can exhibit *bulk* SOTs in addition to the conventional interfacial SOTs enabling magnetization manipulation even in thick single layers without the need for complex multilayer engineering.

The discovery of magnetic van der Waals crystals that retain magnetic order in the two-dimensional limit [1–4] opens up the investigation of their magnetic properties and implementation in spintronic devices. To this end, the efficient control of the magnetic state is essential. Spin-orbit torques (SOTs) provide the opportunity of an electrical control of the magnetization [5]. Linking magnetic van der Waals materials with spin-orbit torques exhibits the potential of current induced magnetization manipulation in two dimensions, thus enabling fast and low power spintronic devices. So far reports of current-induced switching of 2D magnets have been based on interfacial SOTs that rely on complex multilayers requiring a small thickness of the magnetic layer thus limiting thermal stability. [6–8] One of the promising magnetic van der Waals crystals is Fe_3GeTe_2 , which has been shown to exhibit a strong perpendicular magnetocrystalline anisotropy [9], which is still present in an atomic monolayer [10] combined with the Dzyaloshinskii-Moriya interaction stabilizing skyrmions [11–13]. Furthermore, of the van der Waals materials it shows one of the highest bulk Curie temperatures of ~ 225 K [9,14] which can be increased up to room temperature by ionic gating [15].

While switching due to interfacial spin-orbit torques in Fe_3GeTe_2 has been studied in multilayer structures, Johansen et al. [16] recently predicted that a possible bulk SOT could be present due to the symmetry of the monolayer crystalline structure. Since Fe_3GeTe_2 is a metal, the combination of the perpendicular magnetic anisotropy with this theoretically predicted *bulk* SOTs could potentially enable simple new devices: *bulk* SOTs are efficient for thick samples that have a better magnetic thermal stability than the thin flakes necessary for interfacial SOTs, while also drastically simplifying single layer device engineering. However, so far the symmetry analysis has only indicated that *bulk* SOTs are by symmetry allowed [16], but the torques in single Fe_3GeTe_2 layers have not been quantified. Although there have been demonstrations of bulk-type SOTs in 3D magnets such as $L1_0$ FePt and Co-Tb, the origin and the behavior of the SOTs are different from the special *bulk* SOTs that are only present in

materials with particular crystalline structure as studied here in Fe_3GeTe_2 [17,18]. So there is a clear need to check the presence, identify the origin and quantify the amplitude of the torques as key steps forward.

In this work, we fabricate a Fe_3GeTe_2 device with transverse Hall contacts and measure the higher harmonic Hall voltages in order to derive the current induced effective spin-orbit fields. We analyze the symmetries and amplitudes of the torques to understand the bulk and interfacial contributions to the torques and ascertain the temperature dependence highlighting exceptionally large bulk torques in this system.

In a first step, polycrystalline Fe_3GeTe_2 was synthesized from the elements Fe, Ge and Te in a solid-state reaction. A stoichiometric mixture was vacuum-sealed in a quartz glass ampoule, heated up to 625 °C with 100 K/h, and kept at this temperature for 60 hours before cooling to room temperature with 100 K/h. [19] Phase-purity of the gray powder was ensured by X-ray diffraction. In a second step, single crystals of an average size of 1.5 x 1.5 x 0.5 mm³ were grown from the polycrystalline powder via a chemical vapor transport with iodine as the transport agent in a temperature gradient from 750 °C to 700 °C for one week. [20] The atomic structure was verified using high-resolution scanning transmission electron microscopy in Fig. S1a (see also Supplementary Note 1). We confirmed the stoichiometric composition of the Fe_3GeTe_2 by energy dispersive X-ray spectroscopy within an error of about 5% (see Supplementary Note 2). From the grown bulk crystals, Fe_3GeTe_2 flakes were manually exfoliated and placed on an undoped naturally oxidized silicon substrate. The thickness of the flake was measured with an atomic force microscope. By using electron beam lithography, gold contacts were fabricated. The final device can be seen in the inset of Fig. 1a. The flake used in the following study is measured to be 35 nm thick. Assuming the current flows in between the transverse contacts, the cross-section area of the investigated flake is estimated to $A = 1.75 \times 10^{-13} \text{ m}^2$, which is the value used to calculate the current densities.

In order to measure the SOTs, higher harmonic Hall measurements [21] are performed. The measurements were done with the configuration shown in Fig. 1a where the current was applied in the x direction and the Hall voltage U_H was measured in the y direction. The perpendicular magnetic anisotropy of the flake was confirmed by the anomalous Hall measurements for different temperatures as shown in Fig. 1b. While at low temperature abrupt switching is seen, a multi-step switching appears above 175 K near T_c which shows a formation of domains and even skyrmions as observed by TEM in Fig. S4 (see supplementary Note 4). At various temperatures and applied alternating currents j_C , the first (U_H^{1st}) and second harmonic (U_H^{2nd}) Hall voltages are recorded using lock-in amplifiers. For each combination of temperature and current, a magnetic field \mathbf{B} is applied in the plane to tilt the magnetization \mathbf{M} . Thereby, the external field is either aligned with the longitudinal current direction ($\Phi_B = 0^\circ$) or perpendicular to it ($\Phi_B = 90^\circ$). A small z -component prevents multi-domain nucleation, so that the polar angle of the external field ranges between $80^\circ \leq \theta_B \leq 83^\circ$. To take care of heating effects, the second harmonic signal is corrected according to the method outlined in [21].

By consideration of the anomalous and planar Hall effect, the Hall voltage in general can be expressed by [21]:

$$U_H = R_{AHE} j_C \cos(\theta) + R_{PHE} j_C \sin^2(\theta) \sin(2\Phi). \quad (1)$$

R_{AHE} and R_{PHE} are the anomalous and planar Hall effect coefficients and j_C is the applied current.

Expanding equation (1) to first order of the applied current with $j_C = j_0 \cos(\omega t)$ results in:

$$U_H = U_H^{0th} + U_H^{1st} \cos(\omega t) + U_H^{2nd} \cos(2\omega t), \quad (2)$$

$$U_H^{1st} = R_{AHE} j_0 \cos(\theta_0) + R_{PHE} j_0 \sin^2(\theta_0) \sin(2\Phi_0), \quad (3)$$

$$U_H^{0th} = U_H^{2nd} = j_0^2/2 (R_{AHE} - 2 R_{PHE} \cos(\theta_0) \sin(2\Phi_0)) \left. \frac{\partial \cos(\theta)}{\partial B} \right|_{\theta_0} \frac{1}{\sin(\theta_B - \theta_0)} b_{SOT}^\theta +$$

$$j_0^2/2 R_{PHE} \sin^2(\theta_0) \frac{2\cos(2\Phi_0)}{B \sin(\theta_B)} b_{SOT}^\Phi. \quad (4)$$

Here, b_{SOT}^θ and b_{SOT}^Φ are the derivatives of the θ - and Φ -components of the effective spin-orbit fields with respect to the current density and θ_0 and Φ_0 are the equilibrium angles of the

material's magnetization. In the following, we assume that the azimuthal angles of the magnetization and the magnetic field are equal: $\Phi \equiv \Phi_0 = \Phi_B$. Due to the measurement configuration with $\Phi = 0^\circ/90^\circ$, all terms including $\sin(2\Phi_0)$ become zero in equation (3) and (4). In [16] a description of the current induced effective spin-orbit field has been derived in particular for the Fe_3GeTe_2 crystal structure:

$$\mathbf{B}_{\text{SOT}} = \Gamma_0 J_C (m_x \mathbf{e}_x - m_y \mathbf{e}_y). \quad (5)$$

Γ_0 is a parameter, which represents the strength of the spin-orbit torques, J_C is the applied current density, m_i is the i^{th} component of the magnetization unit vector and \mathbf{e}_x and \mathbf{e}_y are the x - and y -unit vectors. We see that these torques lead to a canting of the spins into the plane of the sample and can facilitate switching by reducing the switching energy barrier. The canting lends itself naturally to detection by higher harmonic Hall measurements. By transforming equation (5) to spherical coordinates and considering the measurement configuration $\Phi = 0^\circ/90^\circ$, we find that the spin-orbit field only comprises a θ -component:

$$B_{\text{SOT}}^\theta = \Gamma_0 J_0/2 \sin(2\theta_0) \cos(2\Phi). \quad (6)$$

$J_0 = j_0/A$ is the current density. For this reason, b_{SOT}^Φ in equation (4) is also zero and the first and second harmonic Hall resistances can finally be formulated to:

$$R_{\text{H}}^{1\text{st}} = R_{\text{AHE}} \cos(\theta_0), \quad (7)$$

$$R_{\text{H}}^{2\text{nd}} = j_0/2 R_{\text{AHE}} \left. \frac{\partial \cos(\theta)}{\partial B} \right|_{\theta_0} \frac{1}{\sin(\theta_B - \theta_0)} b_{\text{SOT}}^\theta. \quad (8)$$

Consequently, by measuring $R_{\text{H}}^{2\text{nd}}$, θ_0 and $R_{\text{AHE}} \left. \frac{\partial \cos(\theta)}{\partial B} \right|_{\theta_0} = \left. \frac{\partial R_{\text{H}}^{1\text{st}}}{\partial B} \right|_{\theta_0}$, we derive the current induced effective SOTs b_{SOT}^θ . In Fig. 2 the first and second harmonic Hall resistances after correction for heating effects are plotted as a function of the applied magnetic field when the magnetic field applied in the $\Phi = 0^\circ$ and 90° direction. Note that the field dependence of the second harmonic signal in the $\Phi = 0^\circ$ and 90° configurations is found to be odd and even, respectively.

The next step is to check the nature of the torques by measuring their symmetry. To obtain the polar angular dependence (θ_0), we plot in in Fig. 3a the current-induced effective spin-orbit torques b_{SOT}^θ as a function of the applied magnetic field, which corresponds to a certain polar angle. Data points corresponding to smaller external fields are omitted, due to the fact that the term $\left. \frac{\partial R_{\text{H}}^{\text{1st}}}{\partial B} \right|_{\theta_0}$ diverges near the switching region. In Fig. 3b the same b_{SOT}^θ data is plotted as a function of the extracted polar magnetization angle θ_0 . To demonstrate the odd-symmetry dependence of the damping-like effective field geometry ($\Phi = 0^\circ$) and check that they overlap, we invert the data points corresponding to negative applied fields. The field-like effective field geometry ($\Phi = 90^\circ$) values range between -2 and 4 mT/ 10^{11} Am $^{-2}$ with the highest values at smaller θ_0 angles. The damping-like effective fields decrease in magnitude from -8 to -3 mT/ 10^{11} Am $^{-2}$ with increasing angle. Above $\theta_0 > 45^\circ$ the absolute value of b_{SOT}^θ increases again up to -4 mT/ 10^{11} Am $^{-2}$.

The key step now is to clarify the origin of these torques to check if they are of bulk origin as predicted. A first observed key feature that allows us to identify the bulk origin is the opposite behaviour of the effective spin-orbit fields for $\Phi = 0^\circ$ and $\Phi = 90^\circ$ as predicted by equation (6) due to the $\cos(2\Phi)$ term that yields +1 for $\Phi = 0^\circ$ and -1 for $\Phi = 90^\circ$.

Secondly from the θ_0 dependence we can identify a dominating bulk origin. We can fit equation (6) for pure *bulk* SOTs to the data in Fig. 3b. To check if additionally interfacial torques play a role, the fit equation was extended to take into account an additional interfacial SOTs [21]. Accordingly, we fit our data with a combination of bulk and interfacial SOTs [16,21]:

$$b_{\text{SOT}}^\theta (\Phi = 0^\circ) = \Gamma_0^{\parallel}/2 \sin(2\theta_0) + T_0^{\parallel} + T_2^{\parallel} \sin^2(\theta_0) \quad (9)$$

$$b_{\text{SOT}}^\theta (\Phi = 90^\circ) = -\Gamma_0^{\perp}/2 \sin(2\theta_0) - \cos(\theta_0) (T_0^{\perp} + T_2^{\perp} \sin^2(\theta_0)) \quad (10)$$

Where T_i^\parallel and T_i^\perp are the i^{th} order components of the longitudinal and transverse components of spin-orbit torques from the interface. Fig. 3b shows the resulting fit of the interfacial spin-orbit torques.

To finally check if the key feature of *bulk* SOTs, namely the opposite behavior for $\Phi = 0^\circ$ and $\Phi = 90^\circ$ is universally present or a random occurrence by chance at 175 K (the data shown in Fig. 3), we investigate the temperature dependence. By extracting Γ_0 from each fit, the fundamental magnitude of *bulk* SOTs in Fe_3GeTe_2 can be determined as a function of temperature as shown in Fig. 4. As visible in the temperature dependence, the behavior of $\Gamma_0 \cdot \cos(2\Phi)$ exhibits consistently at all temperatures opposite behavior for $\Phi = 0^\circ$ and $\Phi = 90^\circ$ in line with the prediction for *bulk* SOTs. Note that the fits for Γ_0 were done independently for $\Phi = 0^\circ$ and $\Phi = 90^\circ$ so that one could easily determine if the temperature dependence were qualitatively different for both orientations. However here we see that for both orientations the largest values for Γ_0 occur at the lowest temperatures and then decrease to lower values for temperatures up to 150K before increasing again and peaking around 215 K. Note that the reduction of Γ_0 at even higher temperatures approaching the Curie temperature (230 K) is expected as the magnetic order is lost and at elevated temperature close to the Curie temperature inhomogeneous properties and domain formation can make the analysis less robust. The complex behavior of Γ_0 at elevated temperatures could thus be related to the multi-step switching indicating domain formation shown in Fig. 1b. We note that at higher temperatures the error bars are smaller as the magnetization can be tilted with our maximum available vector field of 5T to higher angles and a wider θ_0 angle range can be investigated and fitted since the anisotropy decreases with temperature.

In particular, the data shows that at low temperatures we measure very high values of b^{θ}_{SOT} of more than $50 \text{ mT}/10^{11} \text{ Am}^{-2}$. Together with the very high interfacial SOTs found in $\text{Fe}_3\text{GeTe}_2/\text{Pt}$ structures [7,8], this bodes well for efficient switching of the magnetization in this material by combined bulk and interfacial torques.

In the following, we discuss the possible origins of the SOTs that we measure. In [16] a SOT mechanism related to a broken inversion symmetry of the structure is introduced. While the polar angular dependences found at the different temperatures indicate a dominating bulk origin of the torques, we see that the temperature dependence does show some deviations from the strict proportionality expected from eq. 6 and the absolute values for $\Phi = 0^\circ$ and $\Phi = 90^\circ$ shown in Fig. 4 do not always fully coincide. This indicates that additional higher order torques that can for instance be induced by uniaxial strain can play a role, highlighting the breadth of new torques that can contribute due to our identified bulk mechanisms. Furthermore, we see that fits of the polar angular dependence (Fig. 3) indicate additional interfacial torques beyond the intrinsic bulk torque can be present. To check why interfacial torques can occur, even though the Fe_3GeTe_2 device that is measured is in principle a bulk device with a thickness of 35 nm, where no net interfacial torques due to the spin Hall effect or the inverse spin-galvanic effect [5,22] are expected, we consider surface oxidation. Overall, this device has been exposed to air < 12 hours and literature reports a natural oxidation layer on an exfoliated flake within a time scale of 14 hours [23,24]. The presence of an oxide layer on the surface exposed to air is confirmed by TEM (see supplementary material fig. S3) and thus interfacial SOTs can appear. So we find that in our Fe_3GeTe_2 device clear evidence for a theoretically reported *bulk* SOT based on the crystal symmetry breaking [16] and on the other hand an additional interfacial SOT are enabled by local surface oxidation. A third possible contribution to the measured spin-orbit torques could be Oersted fields, which are additional magnetic fields, which arise due to the current flow and can mimic a field-like torque symmetry. Assuming that the Fe_3GeTe_2 flake is a homogeneous conductor, the Oersted field is zero in the center of the flake and rises in magnitude at the edges, pointing counterclockwise in the yz -plane [25]. Thus, it points in opposite y -directions at the top and bottom of the flake and cancels to zero. If we assume that the Fe_3GeTe_2 flake has become a heterogeneous conductor due to possible interfaces, the current flow in the z -direction becomes asymmetric and hence also the Oersted field. In the less

conducting areas, this Oersted field can be estimated by $H_{Oe} = \mu_0 j_c / (2\pi r)$ according to the Biot-Savart law for an infinite long straight conductor with r the distance from the conductor. Therefore, exactly at the interfaces to less conducting areas e.g. at the top of the flake the Oersted field becomes maximal. However, given that we probe the bulk of the flake, the contribution of the Oersted field will be negligible compared to the measured torque values.

In order to quantify the *bulk* SOT from a theoretical perspective, we employ the microscopic first-principles framework to compute the anti-damping SOT within the Kubo linear response theory for the Fe_3GeTe_2 bulk crystal (details are given in the Supplementary Note 5). As bulk Fe_3GeTe_2 maintains inversion symmetry the SOT vanishes globally [26]. However, each layer separately may exhibit a non-vanishing SOT which may lead to the non-vanishing effect observed experimentally. If we decompose the unit cell into the A and B layers of Fe_3GeTe_2 (Fig. S4 of the supporting material) the top and bottom Fe atoms of the A-layer experience an equal in magnitude but opposite in sign SOT for an out-of-plane magnetization. However, once the magnetization is tilted away from the out-of-plane direction the SOT for each layer does not cancel out separately. From first principles, the estimated magnitude of the SOT per layer with a magnetization angle of $\theta = 30^\circ$ from the z axis, and $\varphi = 55^\circ$ from the current direction of is $2.19 \text{ mT} / (10^{11} \text{ Am}^{-2})$ and of similar order to that found experimentally (Fig. 3b at $\theta_0=30^\circ$, $\Phi = 55^\circ$).

In summary, we have measured SOTs in a pure Fe_3GeTe_2 flake with very large magnitudes of more than $50 \text{ mT} / 10^{11} \text{ Am}^{-2}$. From a symmetry analysis we can identify the predicted *bulk* SOTs that result from the particular crystalline structure of the Fe_3GeTe_2 that we determine by TEM imaging. In addition, we find that interfacial SOTs are present that result likely from surface effects such as observed oxidation. *Ab initio* calculations confirm that the layer resolved *bulk* SOT is of the same order of magnitude as the experiment. Our findings that the *bulk* SOTs that are a unique property of certain van der Waals materials such as Fe_3GeTe_2 yield very efficient magnetization manipulation due to high effective fields combined with the possibility

of simple device design with just a single material without any additional materials and layers lays the foundations for a new paradigm of 2D materials spin-orbitronic devices.

Acknowledgements

The work at JGU Mainz was funded by the Deutsche Forschungsgemeinschaft (DFG, German Research Foundation) – TRR 173 – 268565370 (projects A01 and B02), the EU (FET-Open grant agreement no. 863155 (s-Nebula), ERC Synergy grant agreement no. 856538 (3D MAGiC), and the Research Council of Norway (QuSpin Center 262633). T.S., D.G., and Y.M. gratefully acknowledge the Jülich Supercomputing Centre for providing computational resources and Deutsche Forschungsgemeinschaft (DFG, German Research Foundation) – TRR 173 – 268565370 (project A11), TRR 288 – 422213477 (project B06).

References

- [1] B. Huang, G. Clark, E. Navarro-Moratalla, D. R. Klein, R. Cheng, K. L. Seyler, D. Zhong, E. Schmidgall, M. A. McGuire, D. H. Cobden, W. Yao, D. Xiao, P. Jarillo-Herrero, and X. Xu, *Layer-Dependent Ferromagnetism in a van Der Waals Crystal down to the Monolayer Limit*, *Nature* **546**, 270 (2017).
- [2] C. Gong and X. Zhang, *Two-Dimensional Magnetic Crystals and Emergent Heterostructure Devices*, *Science* (80-.). **363**, eaav4450 (2019).
- [3] C. Gong, L. Li, Z. Li, H. Ji, A. Stern, Y. Xia, T. Cao, W. Bao, C. Wang, Y. Wang, Z. Q. Qiu, R. J. Cava, S. G. Louie, J. Xia, and X. Zhang, *Discovery of Intrinsic Ferromagnetism in Two-Dimensional van Der Waals Crystals*, *Nature* **546**, 265 (2017).
- [4] M. Gibertini, M. Koperski, A. F. Morpurgo, and K. S. Novoselov, *Magnetic 2D Materials and Heterostructures*, *Nat. Nanotechnol.* **14**, 408 (2019).

- [5] A. Manchon, J. Železný, I. M. Miron, T. Jungwirth, J. Sinova, A. Thiaville, K. Garello, and P. Gambardella, *Current-Induced Spin-Orbit Torques in Ferromagnetic and Antiferromagnetic Systems*, Rev. Mod. Phys. **91**, 35004 (2019).
- [6] V. Ostwal, T. Shen, and J. Appenzeller, *Efficient Spin-Orbit Torque Switching of the Semiconducting Van Der Waals Ferromagnet Cr₂Ge₂Te₆*, Adv. Mater. **32**, 1906021 (2020).
- [7] M. Alghamdi, M. Lohmann, J. Li, P. R. Jothi, Q. Shao, M. Aldosary, T. Su, B. P. T. Fokwa, and J. Shi, *Highly Efficient Spin-Orbit Torque and Switching of Layered Ferromagnet Fe₃GeTe₂*, Nano Lett. **19**, 4400 (2019).
- [8] X. Wang, J. Tang, X. Xia, C. He, J. Zhang, Y. Liu, C. Wan, C. Fang, C. Guo, W. Yang, Y. Guang, X. Zhang, H. Xu, J. Wei, M. Liao, X. Lu, J. Feng, X. Li, Y. Peng, H. Wei, R. Yang, D. Shi, X. Zhang, Z. Han, Z. Zhang, G. Zhang, G. Yu, and X. Han, *Current-Driven Magnetization Switching in a van Der Waals Ferromagnet Fe₃GeTe₂*, Sci. Adv. **5**, eaaw8904 (2019).
- [9] V. Y. Verchenko, A. A. Tsirlin, A. V Sobolev, I. A. Presniakov, and A. V Shevelkov, *Ferromagnetic Order, Strong Magnetocrystalline Anisotropy, and Magnetocaloric Effect in the Layered Telluride Fe_{3-δ}GeTe₂*, Inorg. Chem. **54**, 8598 (2015).
- [10] Z. Fei, B. Huang, P. Malinowski, W. Wang, T. Song, J. Sanchez, W. Yao, D. Xiao, X. Zhu, A. F. May, W. Wu, D. H. Cobden, J.-H. Chu, and X. Xu, *Two-Dimensional Itinerant Ferromagnetism in Atomically Thin Fe₃GeTe₂*, Nat. Mater. **17**, 778 (2018).
- [11] B. Ding, Z. Li, G. Xu, H. Li, Z. Hou, E. Liu, X. Xi, F. Xu, Y. Yao, and W. Wang, *Observation of Magnetic Skyrmion Bubbles in a van Der Waals Ferromagnet Fe₃GeTe₂*, Nano Lett. **20**, 868 (2020).

- [12] Y. Wu, S. Zhang, J. Zhang, W. Wang, Y. L. Zhu, J. Hu, G. Yin, K. Wong, C. Fang, C. Wan, X. Han, Q. Shao, T. Taniguchi, K. Watanabe, J. Zang, Z. Mao, X. Zhang, and K. L. Wang, *Néel-Type Skyrmion in WTe_2/Fe_3GeTe_2 van Der Waals Heterostructure*, Nat. Commun. **11**, 3860 (2020).
- [13] T.-E. Park, L. Peng, J. Liang, A. Hallal, F. S. Yasin, X. Zhang, K. M. Song, S. J. Kim, K. Kim, M. Weigand, G. Schütz, S. Finizio, J. Raabe, K. Garcia, J. Xia, Y. Zhou, M. Ezawa, X. Liu, J. Chang, H. C. Koo, Y. D. Kim, M. Chshiev, A. Fert, H. Yang, X. Yu, and S. Woo, *Néel-Type Skyrmions and Their Current-Induced Motion in van Der Waals Ferromagnet-Based Heterostructures*, Phys. Rev. B **103**, 104410 (2021).
- [14] N. León-Brito, E. D. Bauer, F. Ronning, J. D. Thompson, and R. Movshovich, *Magnetic Microstructure and Magnetic Properties of Uniaxial Itinerant Ferromagnet Fe_3GeTe_2* , J. Appl. Phys. **120**, 83903 (2016).
- [15] Y. Deng, Y. Yu, Y. Song, J. Zhang, N. Z. Wang, Z. Sun, Y. Yi, Y. Z. Wu, S. Wu, J. Zhu, J. Wang, X. H. Chen, and Y. Zhang, *Gate-Tunable Room-Temperature Ferromagnetism in Two-Dimensional Fe_3GeTe_2* , Nature **563**, 94 (2018).
- [16] Ø. Johansen, V. Risinggård, A. Sudbø, J. Linder, and A. Brataas, *Current Control of Magnetism in Two-Dimensional Fe_3GeTe_2* , Phys. Rev. Lett. **122**, 217203 (2019).
- [17] J. W. Lee, J. Y. Park, J. M. Yuk, and B.-G. Park, *Spin-Orbit Torque in a Perpendicularly Magnetized Ferrimagnetic Tb-Co Single Layer*, Phys. Rev. Appl. **13**, 44030 (2020).
- [18] S. Q. Zheng, K. K. Meng, Q. B. Liu, J. K. Chen, J. Miao, X. G. Xu, and Y. Jiang, *Disorder Dependent Spin–Orbit Torques in $L10$ FePt Single Layer*, Appl. Phys. Lett. **117**, 242403 (2020).

- [19] H.-J. Deiseroth, K. Aleksandrov, C. Reiner, L. Kienle, and R. K. Kremer, *Fe₃GeTe₂ and Ni₃GeTe₂ – Two New Layered Transition-Metal Compounds: Crystal Structures, HRTEM Investigations, and Magnetic and Electrical Properties*, Eur. J. Inorg. Chem. **2006**, 1561 (2006).
- [20] B. Chen, J. Yang, H. Wang, M. Imai, H. Ohta, C. Michioka, K. Yoshimura, and M. Fang, *Magnetic Properties of Layered Itinerant Electron Ferromagnet Fe₃GeTe₂*, J. Phys. Soc. Japan **82**, 124711 (2013).
- [21] K. Garello, I. M. Miron, C. O. Avci, F. Freimuth, Y. Mokrousov, S. Blügel, S. Auffret, O. Boulle, G. Gaudin, and P. Gambardella, *Symmetry and Magnitude of Spin–Orbit Torques in Ferromagnetic Heterostructures*, Nat. Nanotechnol. **8**, 587 (2013).
- [22] A. Manchon and A. Belabbes, *Chapter One - Spin-Orbitronics at Transition Metal Interfaces*, in edited by R. E. Camley and R. L. B. T.-S. S. P. Stamps, Vol. 68 (Academic Press, 2017), pp. 1–89.
- [23] D. Kim, S. Park, J. Lee, J. Yoon, S. Joo, T. Kim, K. Min, S.-Y. Park, C. Kim, K.-W. Moon, C. Lee, J. Hong, and C. Hwang, *Antiferromagnetic Coupling of van Der Waals Ferromagnetic Fe₃GeTe₂*, Nanotechnology **30**, 245701 (2019).
- [24] T.-E. Park, L. Peng, J. Liang, A. Hallal, F. Sami Yasin, X. Zhang, S. Jong Kim, K. M. Song, K. Kim, M. Weigand, G. Schuetz, S. Finizio, J. Raabe, K. Garcia, J. Xia, Y. Zhou, M. Ezawa, X. Liu, J. Chang, H. C. Koo, Y. Duck Kim, M. Chshiev, A. Fert, H. Yang, X. Yu, and S. Woo, *Néel-Type Skyrmions and Their Current-Induced Motion in van Der Waals Ferromagnet-Based Heterostructures*, arXiv:1907.01425.
- [25] P. Ho, J. Zhang, D. C. Bono, J. Chen, and C. A. Ross, *Oersted Field and Spin Current Effects on Magnetic Domains in [Co/Pd]15 Nanowires*, IEEE Trans. Magn. **52**, 1 (2016).

- [26] K. Zhang, S. Han, Y. Lee, M. J. Coak, J. Kim, I. Hwang, S. Son, J. Shin, M. Lim, D. Jo, K. Kim, D. Kim, H.-W. Lee, and J.-G. Park, *Gigantic Current Control of Coercive Field and Magnetic Memory Based on Nanometer-Thin Ferromagnetic van Der Waals Fe_3GeTe_2* , *Adv. Mater.* **33**, 2004110 (2021).

Fig. 1. (a) Scheme of the 2nd harmonic Hall measurement. An alternating current is injected along the x -direction, while the transverse 1st and 2nd harmonic Hall voltage U_{trans} is measured via a lock-in amplifier. In the inset an optical microscope image of the final device is depicted. (b) The hysteresis loops of Fe_3GeTe_2 at different temperatures with the magnetic field applied in the z direction.

Fig. 2. Examples of the 1st and 2nd harmonic Hall resistances as a function of the applied magnetic field along the x -direction $\Phi = 0^\circ$ (a) and y -direction $\Phi = 90^\circ$ (b) at a temperature of 100 K with a polar magnetic field angle of $\theta_B = 82^\circ$. The applied current density is $4.1 \times 10^{10} \text{ Am}^{-2}$.

Fig. 3. The derivative of the θ component of the current induced effective field is shown as a function of the externally applied magnetic field (a) and the polar magnetization angle θ_0 (b) at a temperature of 175 K with a polar magnetic field angle of $\theta_B = 82^\circ$. The applied current density is $3.7 \times 10^{10} \text{ Am}^{-2}$. In (b) the data for $\Phi = 0^\circ$ and negative applied fields has been inverted. The solid lines are fits according to equation (9) and (10).

Fig. 4. The extracted *bulk* spin-orbit torque parameter $\Gamma_0 * \cos(2\Phi)$ as a function of the temperature showing the opposite sign for the $\Phi = 0^\circ$ and $\Phi = 90^\circ$ data over the full temperature range.

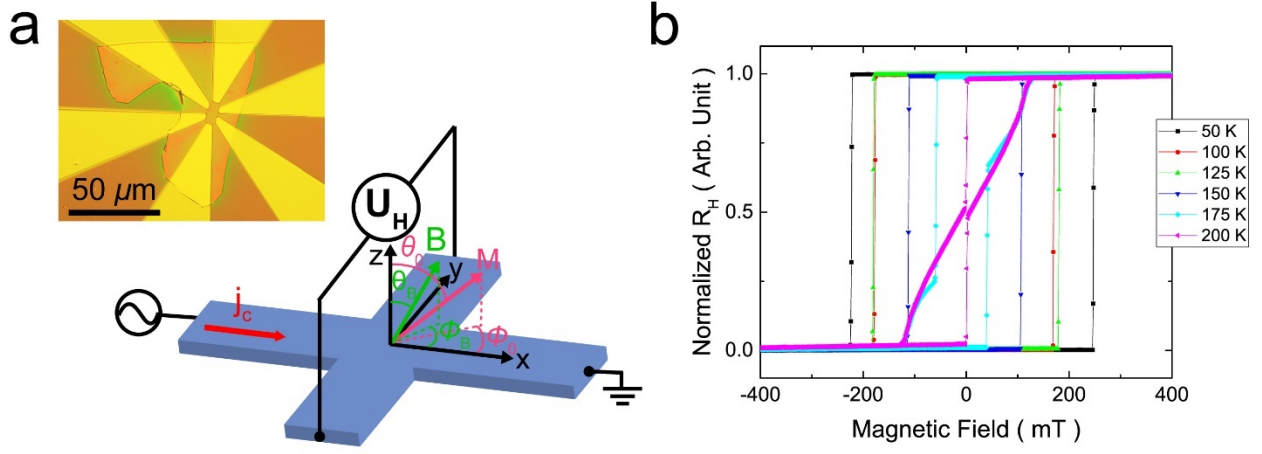


Figure 1

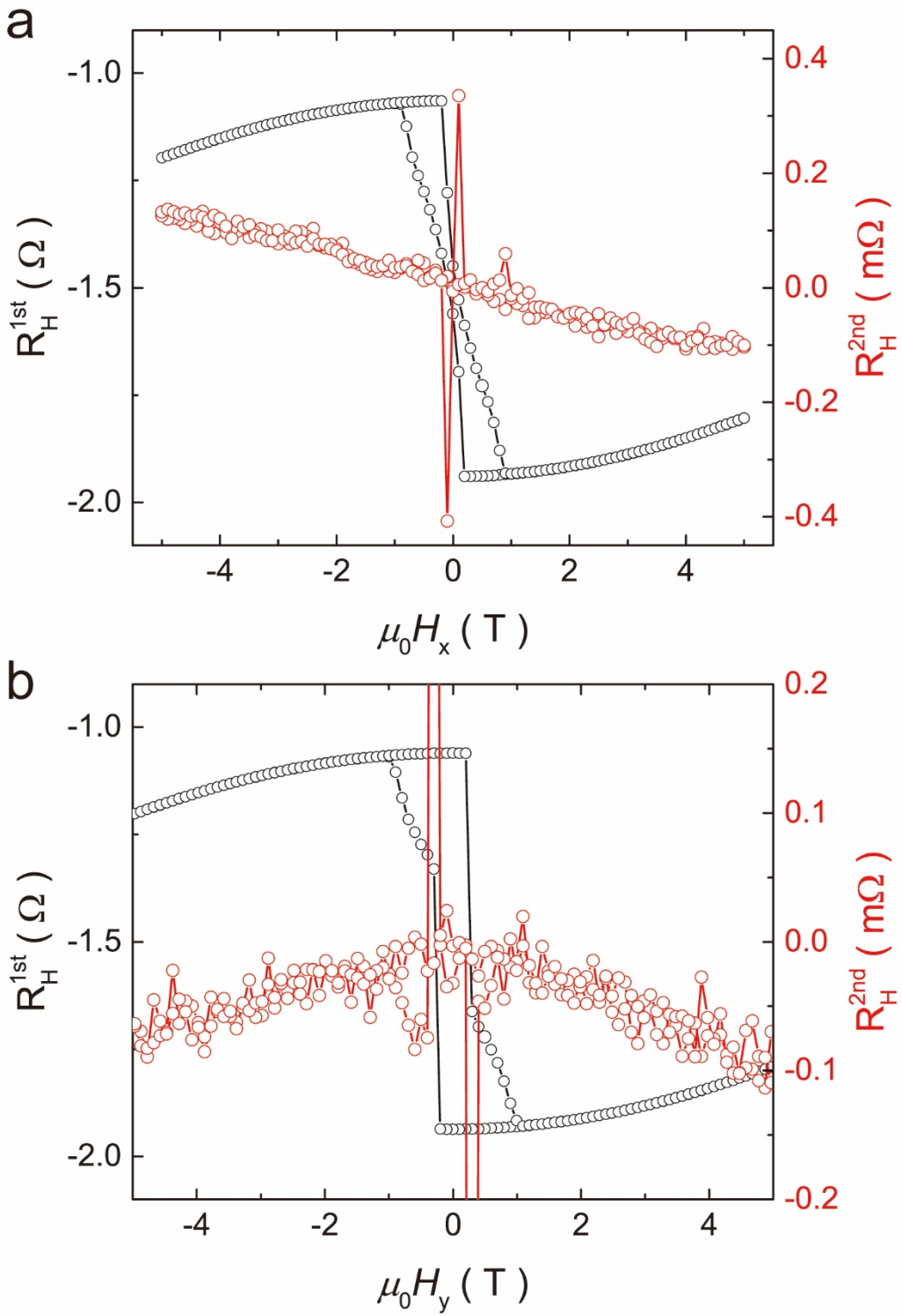


Figure 2

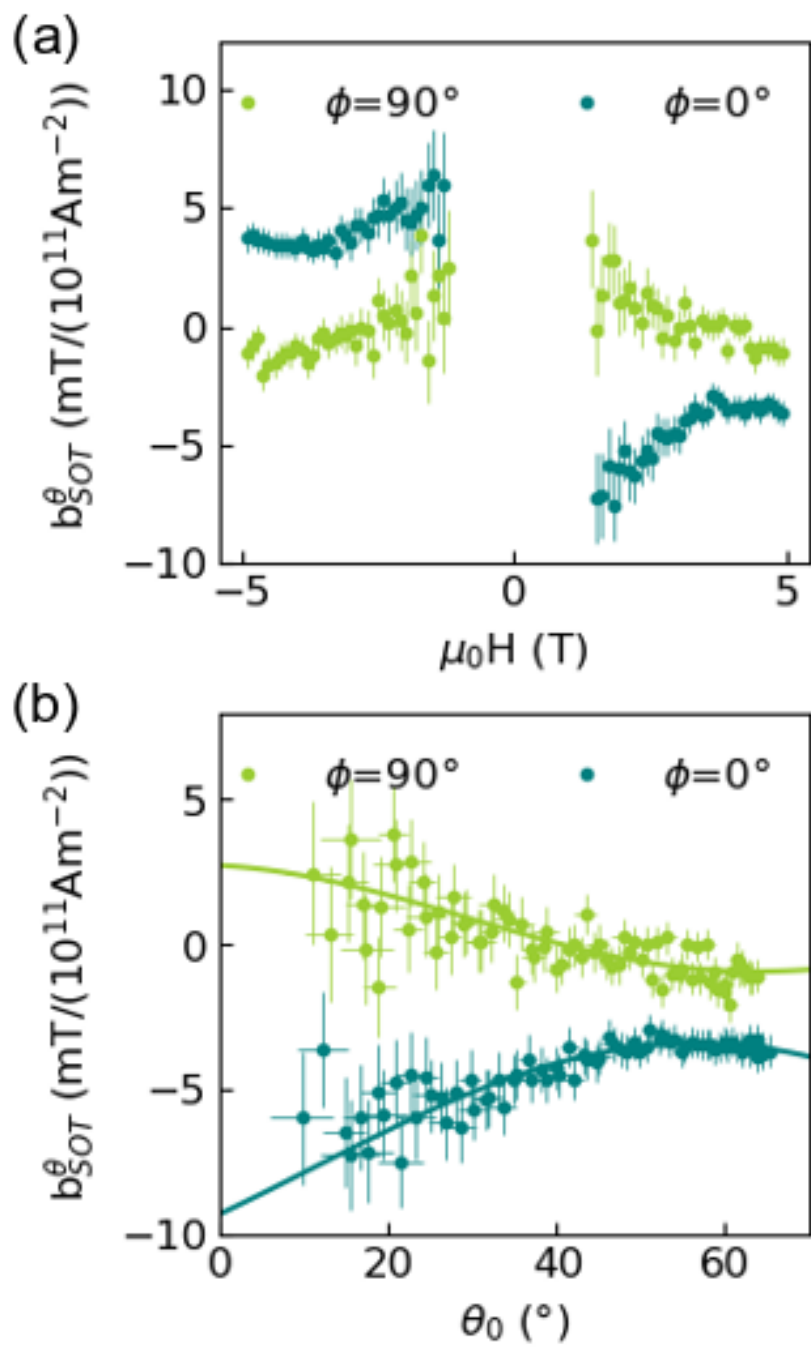


Figure 3

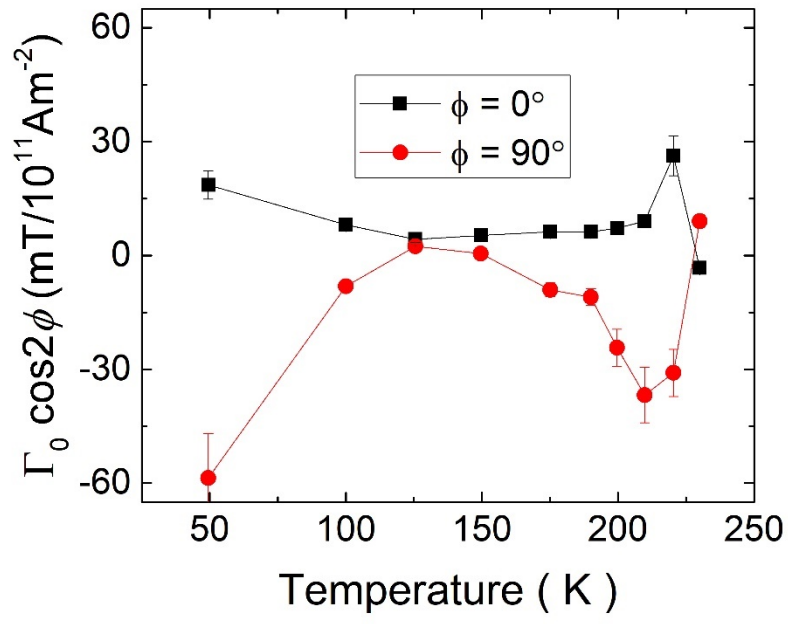


Figure 4